Structural Engineering and Mechanics, *Vol. 62, No. 1 (2017) 85-95*
DOI: https://doi.org/10.12989/sem.2017.62.1.085

Form-finding analysis of suspension bridges using an explicit Iterative approach

Hongyou Cao[1a], Yun-Lai Zhou[*1], Zhijun Chen[2b] and Magd Abdel Wahab[**3,4,5]

[1]*Department of Civil and Environmental Engineering, National University of Singapore, 117576, Singapore*
[2]*School of Civil Engineering & Mechanics, Huazhong University of Science & Technology, Wuhan, 4300743, China*
[3]*Division of Computational Mechanics, Ton Duc Thang University, Ho Chi Minh City, Vietnam*
[4]*Faculty of Civil Engineering, Ton Duc Thang University, Ho Chi Minh City, Vietnam*
[5]*Soete Laboratory, Faculty of Engineering and Architecture, Ghent University, Technologiepark Zwijnaarde 903, B-9052 Zwijnaarde, Belgium*

(Received September 19, 2016, Revised December 16, 2016, Accepted January 23, 2017)

Abstract. This paper presents an explicit analytical iteration method for form-finding analysis of suspension bridges. By extending the conventional analytical form-finding method predicated on the elastic catenary theory, two nonlinear governing equations are derived for calculating the accurate unstrained lengths of the entire cable systems both the main cable and the hangers. And for the gradient-based iteration method, the derivation of explicit calculation for the Jacobian matrix while solving the nonlinear governing equation enhances the computational efficiency. The results from sensitivity analysis show well performance of the explicit Jacobian matrix compared with the traditional finite difference method. According to two numerical examples of long span suspension bridges studied, the proposed method is also compared with those reported approaches or the fundamental criterions in suspension bridge structural analysis, which eventually confirms the accuracy and efficiency of the proposed approach.

Keywords: form-finding analysis; suspension bridge; analytical method; elastic catenary cable; finite element analysis

1. Introduction

Suspension bridges analysis requires a form-finding analysis prior to the finite element (FE) model to determine the geometric parameters and the initial force of the cable system since the configuration of a cable is arbitrary in stress-free state and its stiffness is derived from the applied external loads in contrast to the frame structures (Irvine 1981). In the past years, many numerical and analytical form-finding approaches have evolved for the tensegrity structures (Zhang *et al*. 2014, Koohestani and Guest 2013, Faroughi *et al*. 2014) and the suspension bridges (Sun *et al*. 2014, 2016, Kim *et al*. 2014, Jung *et al*. 2015) as well.

The form-finding analysis methods for suspension bridges can be summarized into three categories: 1) the simplified approach; 2) the FE-based method; and 3) the analytical method. The simplified method assumes the main cable to be a parabola under uniform load along its span direction (Chen *et al*. 2014, Gimsing and Georgakis 2011, Lonetti and Pascuzzo 2014). However, the accuracy of the simplified approximation is insufficient since the main cable sustains both self-weight along its length and concentrated forces from the hangers. The FE-based method identifies the target cable shape by updating the nodal positions and/or initial force of the cable elements according to the nonlinear structural analysis results based on an assumed initial suspension bridge model. Wang and Yang (1996) proposed a successive substitution approach, which predicates on the Newton-Raphson method and modifies the initial tension of the cable elements, to minimize vertical deformation and/or bending moment of the girder under dead load. Karoumi (1999) utilized the trial-and-error procedure for the form-finding analysis of suspension bridges. Like the simplified method, these approaches also assume that the configuration of main cable follows a parabolic shape and fix the nodal position during the iteration process. However, the final configuration of the main cable is not a parabola rigorously. To overcome these drawbacks, several methods, such as the target configuration under dead load (TCUD) method (Kim and Lee 2001) , the initial force method (Kim *et al.* 2002), the improved TCUD (I.TCUD) method (Kim and Kim 2012), the G.TCUD method (Jung *et al.* 2013) and the coordinate iteration method (Sun *et al.* 2014), have been developed successively. These methods find out the target profile of the bridge by treating the nodal positions of the main cable and/or the unstrained length of the bridge's members, e.g., the main cable, the pylon and the girder as variables and solve them in NFEM iteration formula with additional constraints derived from bridge's geometric requirements under dead load. However, the convergence of these FE-

∗Corresponding author, Ph.D.
E-mail: zhouyunlai168168@gmail.com
∗∗Corresponding author, Professor
E-mail: magd.abdelwahab@tdt.edu.vn, magd.abdelwahab@ugent.be
[a]Research Fellow
[b]Professor

ISSN: 1225-4568 (Print), 1598-6217 (Online)

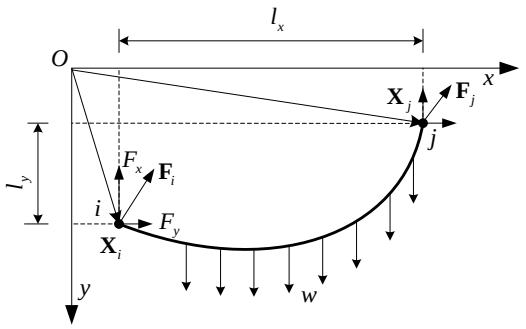

Fig. 1 Two-dimensional catenary cable

based approaches highly depend on the assumed initial FE model (Wriggers 2008).

The analytical approaches, which separates the bridge into two substructures: the cable system and the pylon-girder, couples them via the hanger forces and deals with the cable system independently using analytical method, possess a much higher computational efficiency and faster convergence in contrast to the simplified and the FE-based methods. Based on the elastic catenary equations, O'Brien and his co-workers (1964, 1967) proposed a successive calculation procedure that divides the cable into segments at the positions of the concentrated loads and solves the static equilibrium to determine the cable configuration. This method is mainly used to predict the accurate cable configuration of the suspension bridges during the hanger installation process (Chen *et al*. 2015, Fan *et al*. 1999, Luo 2004) since it requires the unstrained length of each cable element known as prior. Chen *et al*. (2013) improved this method to the form-finding analysis of the suspension under bridge finished stage through considering the unstrained length instead of the horizontal distance of the cable element (the space between the two adjacent hangers) as variables. Wang *et al.* (2015) extended this approach to the preliminary analysis of self-anchored suspension bridge while neglecting the self-weight of the hangers in their main cable analysis model. Similar to above approaches, Jung *et al*. (2015), proposed a simplified analytical method for the optimization of the initial shape analysis in self-anchored suspension bridges. This approach assumes the main cable segments between hangers to be parabolic under self-weight instead of the elastic catenary element. In essence, the analytical form-finding procedure becomes solving a series of implicit nonlinear governing equations derived from the cable system.

The Netwon-Raphson iteration method is the most widely used and efficient approach to solve the nonlinear equations. However, the numerical methods, e.g., finite difference method (FDM), has to be adopted to approximate the Jacobian matrix during the governing equations resolving process due to the implicit expression of the equations (Chen *et al*. 2013, Luo 2004). Although the FDM is simple in application, both truncation and round-off errors that it often suffers will heavily affect the Jacobian matrix approximation quality (Lund 1994). An explicit Jacobian matrix estimation method will not only overcome these defects but also improve the current analytical methods for form-finding analysis of suspension bridge. This study extends the elastic catenary theory based analytical form-finding method to be capable of calculating the accurate unstrained length of the entire cable system, including both main cable and hangers. The Jacobian matrix for the iteration process is derived in explicit form in accordance to the differential form of elastic catenary equations and then sensitivity analysis is carried out to validate the reliability of this explicit method in comparison with FDM. Finally, two long span suspension bridges are numerically studied, and the results are also compared with those existing approaches.

2. Iterative approach for form-finding analysis

This section introduces the elastic catenary theory based analytical form-finding analysis approach for suspension bridges (Chen, Cao, and Zhu 2013). This approach includes the entire cable system information (main cable and hangers) into the governing equations.

2.1 Elastic catenary equations

The elastic catenary theory assumes a perfectly flexible cable with self-weight uniformly distributed along its length as shown in Fig. 1, where $\mathbf{x}_i$ and $\mathbf{x}_j$ denote the coordinates of node *i* and *j*, $\mathbf{F}_i$ and $\mathbf{F}_j$ refer to the nodal forces at both ends, respectively. The elastic catenary equations follow

$$\mathbf{x}_j - \mathbf{x}_i = [l_x, l_y]^T = \boldsymbol{\varphi}(\mathbf{F}_i, L_0) \tag{1}$$

$$\mathbf{F}_j = -\mathbf{F}_i + \mathbf{w}L_0 \tag{2}$$

where L_0 represents the unstrained length of element, $\mathbf{w}=[0,w]^T$, w means the self-weight per length unit of the cable. The two components of $\boldsymbol{\varphi}$ are given in Eqs. (3) and (4) as follows

$$\begin{aligned}\varphi_x = -\frac{F_x L_0}{EA} - \frac{F_x}{w}\Bigg\{&\ln\left[\sqrt{F_x^2 + \left(wL_0 - F_y\right)^2} + wL_0 - F_y\right] \\ &-\ln\left(\sqrt{F_x^2 + F_y^2} - F_y\right)\Bigg\}\end{aligned} \tag{3}$$

$$\varphi_y = -\frac{F_y L_0}{EA} + \frac{wL_0^2}{2EA} + \frac{1}{w}\left[\sqrt{F_x^2 + \left(wL_0 - F_y\right)^2} - \sqrt{F_x^2 + F_y^2}\right] \tag{4}$$

where E and A denote the elastic modulus and the cross-sectional area of the cable, respectively.

2.2 Governing equations

Form-finding analysis is an inverse problem determining the nodal positions and cable tensions or unstrained lengths according to the predetermined geometric parameters of the bridge under the dead load state. The following steps detail the analytical form-finding analysis procedure,

(1) Dividing the bridge into two sub-structures coupled by the hanger forces. As shown in Fig. 2(a), l_s and l_m denote the span of side-span and main-span,

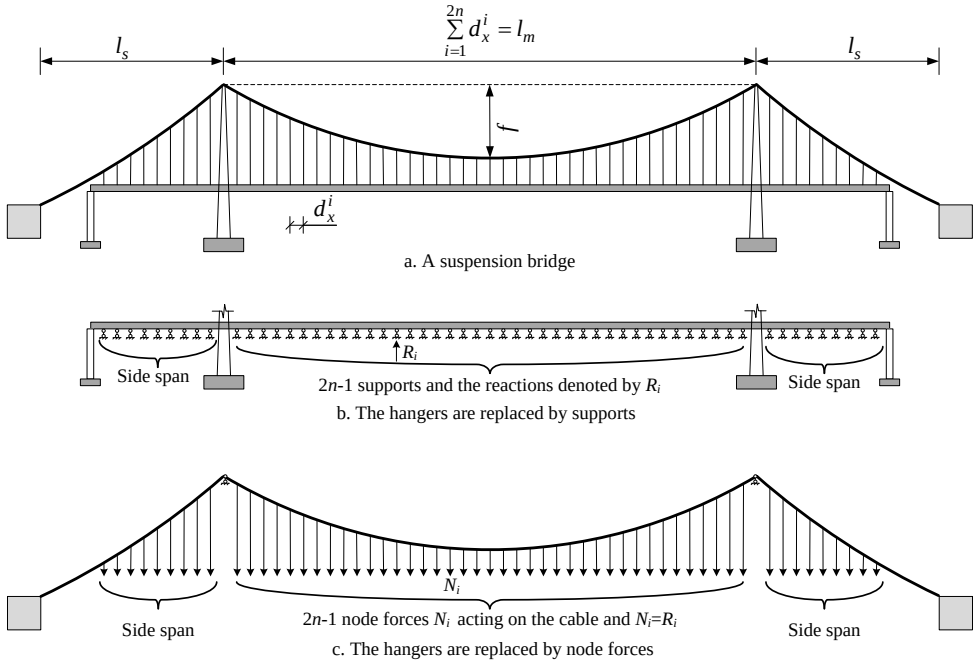

Fig. 2 Structural decomposition of the girder-tower system and cable system

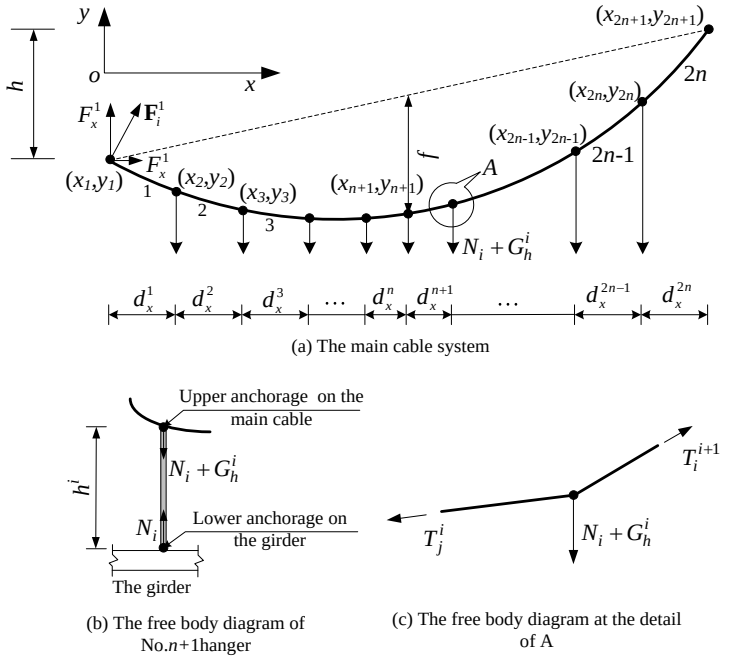

Fig. 3 The main cable system and free body diagrams of the connecting points between girder, hanger and main cable

respectively. f refers to the sag at the mid-span of main cable and d_x^i means the horizontal distance between the i^{th} and the $(i\text{-}1)^{th}$ hangers.

(2) Replacing the hangers by vertical supports and calculating the support forces R_i (i denotes the i^{th} support) according to the target shape of the stiffening girder under dead load as shown in Fig. 2(b). By this way, the hanger forces acting on the stiffening girder N_i (i refers to the i^{th} hanger) are eventually determined by R_i+N_i=0. The force acting on the main cable equals the summation of N_i and the self-weight of the hanger. The structural parameters such as spans, the layout of the hangers and the sag-span ratio are usually determined prior.

(3) Calculating the hanger forces at the lower anchored points, N_i, using the pylon-girder substructure. The cable system thus can be considered as an independent system as shown in Fig. 2(c).

Fig. 3 illustrates the mechanical sketch of the cable system. $\mathbf{F}_i^1 = \left[F_x^1, F_y^1\right]^T$ (the subscript and superscript of **F** denote the left/right node of the cable element and the

element number, respectively) denotes the nodal forces of node *i* of the first cable element. Recalling the elastic catenary element equations Eqs. (1)-(4), the coordinate and nodal forces of node *j* for the first cable element become

$$\mathbf{x}_2 = \mathbf{x}_1 + \left[d_x^1, d_y^1 \right]^T \tag{5}$$

$$\mathbf{F}_j = -\mathbf{F}_i + \mathbf{w}L_0 \tag{6}$$

where, $L_0^1 = \varphi_x^{-1}\left(F_x^1, F_y^1, d_x^1\right)$, $d_y^1 = \varphi_y\left(F_x^1, F_y^1, L_0^1\right)$.

As shown in Fig. 3(b), h_i (*i* represents the i^{th} hanger, *i*=1~2*n*-1) denotes the length of the hanger with elongation. Assuming h_0^i defines the unstrained length of the i^{th} hanger, and the following equations describe the relationship between h_i and h_0^i

$$\int_0^{h_0^i} \frac{N_i + w_h x}{E_h A_h} dx + h_0^i = h^i \tag{7}$$

$$h_0^i = \frac{-\left(N_i + E_h A_h\right) + \sqrt{\left(N_i + E_h A_h\right)^2 + 2E_h w_h A_h h^i}}{w_h} \tag{6}$$

where w_h refers to the weight of the hanger per length unit, E_h and A_h represent the modulus of elasticity and the cross sectional area of the hangers, respectively. The self-weight of i^{th} hanger G_h^i becomes:

$$G_h^i = w_h h_0^i \tag{9}$$

According to the equilibrium condition at i^{th} node as shown in Fig. 3(c), the tension at node *j* of i^{th} element and the tension at *i* node of $(i+1)^{\text{th}}$ element lead to

$$T_j^i = \sqrt{\left(F_x^i\right)^2 + \left(F_y^i - wL_0^i\right)^2} \tag{10}$$

$$T_i^{i+1} = \sqrt{\left(F_x^i\right)^2 + \left(F_y^i - wL_0^i - N_i - G_h^i\right)^2} \tag{11}$$

The force relationship between j^{th} node of i^{th} element and i^{th} node of $(i+1)^{\text{th}}$ element expresses as

$$\mathbf{F}_i^i = \mathbf{F}_i^{i-1} - \mathbf{w}L_0^{i-1} - \mathbf{N}_{i-1} \tag{12}$$

where $\mathbf{N}_{i-1} = [0, N_{i-1} + G_h^{i-1}]^T$, *i*=2~2*n*.

If the nodal force at node *i* of the first cable element, $\mathbf{F}_i^1 = \left[F_x^1, F_y^1\right]^T$, is known, calculating the coordinate and nodal force of each element from 1 to 2*n* successively with Eqs. (5)-(6) and Eq. (12), the coordinate of mid-node and the end node of the main cable can be obtained as

$$\mathbf{x}_{n+1} = \mathbf{x}_1 + \sum_{i=1}^{n}\left[d_x^i, d_y^i \right]^T = \mathbf{x}_1 + \sum_{i=1}^{n}\left[d_x^i, \varphi_y\left(F_x^i, F_y^i, L_0^i\right) \right]^T \tag{13}$$

$$\mathbf{x}_{2n+1} = \mathbf{x}_1 + \sum_{i=1}^{2n}\left[d_x^i, d_y^i \right]^T = \mathbf{x}_1 + \sum_{i=1}^{2n}\left[d_x^i, \varphi_y\left(F_x^i, F_y^i, L_0^i\right) \right]^T \tag{14}$$

According to the structural parameters of the bridge, such as span, sag and the relative height between the neighbouring pylons, the coordinates of the main cable at mid-span and the end are known and can be expressed as

$$\mathbf{x}_{n+1} = \mathbf{x}_1 + \left[l/2, h/2 - f \right]^T \tag{15}$$

$$\mathbf{x}_{2n+1} = \mathbf{x}_1 + \left[l, h \right]^T \tag{16}$$

where *l* denotes the span of the bridge, *f* refers to the mid-span sag of the main cable and *h* represents the relative height between neighboring pylons as shown in Fig. 3(a).

With Eqs. (13)-(16) and substituting the expression of L_0^i into the equations, the governing equations of form-finding method for a plane-shape cable becomes

$$\begin{aligned}&\left[\sum_{i=1}^{n} \varphi_y\left(F_x^i, F_y^i, \varphi_x^{-1}\left(F_x^i, F_y^i, d_x^i\right)\right), \sum_{i=1}^{2n} \varphi_y\left(F_x^i, F_y^i, \varphi_x^{-1}\left(F_x^i, F_y^i, d_x^i\right)\right) \right]^T \\ &= \left[d_y^{n+1}, d_y^{2n+1} \right]^T = \left[h/2 - f, h \right]^T\end{aligned} \tag{17}$$

2.3 Nonlinear iteration procedure

The following gradient-based iteration method is employed to solve Eq. (17),

Step 1: Assuming the main cable shape follows a parabola under dead load, the initial iteration forces, $\mathbf{F}_i^1 = [F_x^1, F_y^1]^T$, can be estimated by the following equations

$$F_x^1 = \frac{q_d l^2}{8f} + \left(1 + \frac{8f^2}{3l^2}\right)\frac{q_m l^2}{8f} \tag{18}$$

$$F_y^1 = F_x^1 \tan\theta = F_x^1 \frac{(h - 4f)}{l} \tag{19}$$

where, q_d and q_m are the dead load and self-weight per unit length of stiffening girder and main cable, respectively.

Step 2: Calculating the unstrained length of the first element, L_0^1, and the nodal coordinate, (x_2, y_2), and the force, $\mathbf{F}_j^1$, of node *j* according to Eqs. (1)-(2).

Step 3: Calculating the node *i* forces, $\mathbf{F}_i^2 = [F_x^2, F_y^2]^T$, of the second element according to Eq. (12), and calculating the unstrained length of the second element, L_0^2, the nodal coordinate, (x_3, y_3), and the forces, $\mathbf{F}_j^2$ according to Eqs. (1)-(2). Repeating this procedure until all the cable elements' nodal coordinates and forces are calculated.

Step 4: calculating d_y^{n+1} and d_y^{2n+1} according to the *y*-direction coordinate of node 1, *n*+1 and 2*n*+1, and checking the convergence of the iteration procedure using the following convergence criteria

$$R = \sqrt{\left(\frac{d_x^{n+1} - d_{x,m}^{n+1}}{d_x^{n+1}}\right)^2 + \left(\frac{d_x^{2n+1} - d_{x,m}^{2n+1}}{d_x^{2n+1}}\right)^2} \le \varepsilon \tag{20}$$

where, $d_{x,m}^{n+1} = h/2 - f$, $d_{x,m}^{2n+1} = h$, and ε is the tolerance defined by users. If the convergence criterion is satisfied, terminate the iteration, or else go to the **Step 5**.

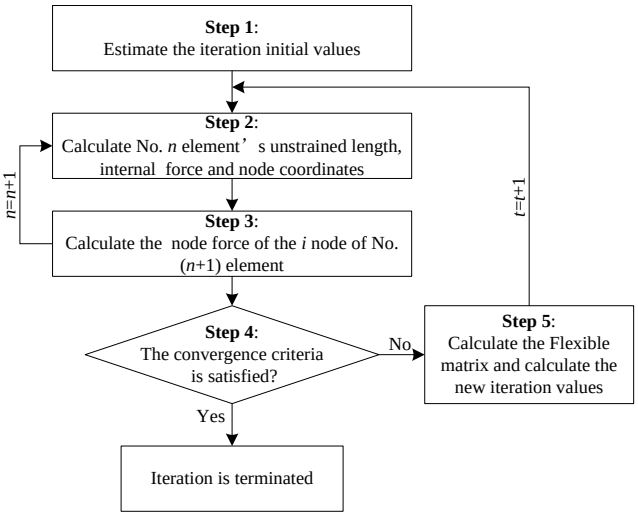

Fig. 4 The flow chart of the flexible iteration procedure

Step 5: If the convergence criteria in Eq. (20) is not achieved, the following iteration formula is adopted

$$\begin{bmatrix} d_{x,m}^{n+1} \\ d_{x,m}^{2n+1} \end{bmatrix} = \begin{bmatrix} d_{x}^{n+1,t} \\ d_{x}^{2n+1,t} \end{bmatrix} + [\mathbf{J}]_{2\times 2} \Delta \mathbf{F}_i^{1,t} \tag{21}$$

where, t denotes the iteration step. $\Delta \mathbf{F}_i^{1,t}$ can be expressed as

$$\Delta \mathbf{F}^{1,t} = [\mathbf{J}]_{2\times 2}^{-1} \begin{bmatrix} d_{x,m}^{n+1} - d_{x}^{n+1,t} \\ d_{x,m}^{2n+1} - d_{x}^{2n+1,t} \end{bmatrix} \tag{22}$$

and $\mathbf{F}_i^{1,t+1}$ for the next iteration step t+1 is

$$\mathbf{F}_i^{1,t+1} = \mathbf{F}_i^{1,t} + \Delta \mathbf{F}_i^{1,t} \tag{23}$$

Finally, go back to **Step 2** for the next iteration step.

The matrix shown in Eq. (21) is called flexible matrix indicating the relationship between the vector function, $\boldsymbol{\varphi} = \left[d_y^{n+1}, d_y^{2n+1} \right]^T$, and the vector variable, $\mathbf{F}_i^{1,t}$ from mathematical viewpoint. Because function $\boldsymbol{\varphi}$ expresses in an implicit form, the gradient matrix, [**J**], usually is approximated by FDM.

The FDM approximates the derivative of the response based on the response function values

$$\frac{\partial \varphi_i}{\partial x_j} \approx \frac{\varphi_i\left(\mathbf{x} + \Delta x_j \mathbf{e}_j\right) - \varphi_i(\mathbf{x})}{\Delta x_j} \tag{24}$$

Δx_j is a small perturbation applied to the j^{th} design variable x_j, and $\mathbf{e}_j$ is a vector unit in the j^{th} direction. One additional function evaluation is need for every design variable x_j to compute the full gradient. Even though, this method is straightforward and can be easily implemented for any response function, the approximation quality strongly depends on the step size Δx_j, which is an obvious inherent drawback of this method. Both truncation and round-off errors are present in FDM. Truncation errors are due to the terms disregarded in the Taylor expansion in Eq. (24). A smaller perturbation Δx_j will reduce this error. In contrast, round-off errors increase strongly when Δx_j is very small. Therefore, a compromise between both types of errors is required during application of FDM.

Fig. 4 gives the flowchart for the flexible iteration procedure. The TCUD of the main cable in the main span is obtained under the hypothesis that the tower is in zero-bending moment state under dead load which means the horizontal component of the side main cable tension equals to that of the main cable. When calculating the TCUD of the main cable in the side span, the first term in Eq. (17) can be removed, and the governing equation of the form-finding analysis for side span is reduced as a single variable nonlinear equation. The calculation procedure for side span is also the same as the flowchart shown in Fig. 4 with the horizontal component of $\mathbf{F}_i^1$ as known.

3. Jacobian matrix derivation and sensitivity analysis

This section derives an explicit gradient matrix formula from the recursion relation in Eq. (12) and the differential form of elastic catenary equations to overcome the shortcomings of FDM. A sensitivity analysis is also conducted to verify the feasibility and efficiency.

3.1 Jacobian matrix derivation

According to the flexible iteration procedure, substituting Eq. (12) into Eq. (17) leads to a form only respecting to variables $\mathbf{F}_i^1 = \left[F_x^1, F_y^1 \right]^T$.

$$\begin{aligned} &\left[\sum_{i=1}^{n} \varphi_y\left(F_x^1, F_y^1, \varphi_x^{-1}\left(F_x^1, F_y^1, d_x^i\right)\right), \sum_{i=1}^{2n} \varphi_y\left(F_x^1, F_y^1, \varphi_x^{-1}\left(F_x^1, F_y^1, d_x^i\right)\right) \right]^T \\ &= \left[d_y^{n+1}, d_y^{2n+1} \right]^T = \left[h/2 - f, h \right]^T \end{aligned} \tag{25}$$

Assuming function **U** as

$$\mathbf{U} = \begin{bmatrix} d_y^{n+1} - h/2 + f \\ d_y^{2n+1} - h \end{bmatrix} \tag{26}$$

Linearizing the nonlinear function **U** by first-order Taylor expansion at $\left(\mathbf{F}_m^1, \cdots, \mathbf{F}_m^{2n}\right)$, and then

$$\mathbf{U} = \mathbf{U}\left(\mathbf{F}_m^1, \cdots, \mathbf{F}_m^{2n}\right) + \begin{bmatrix} \mathbf{C}_1 & \cdots & \mathbf{C}_n & \mathbf{0} & \mathbf{0} \\ \mathbf{C}_1 & \cdots & \mathbf{C}_n & \cdots & \mathbf{C}_{2n} \end{bmatrix} \begin{bmatrix} \Delta \mathbf{F}_m^1 \\ \vdots \\ \Delta \mathbf{F}_m^{2n} \end{bmatrix} \tag{27}$$

where,

$$\mathbf{C}_i = \left[\frac{\partial \varphi_y\left(F_x^i, F_y^i, I_0^i\right)}{\partial F_x^i}, \frac{\partial \varphi_y\left(F_x^i, F_y^i, I_0^i\right)}{\partial F_y^i} \right]$$

$$\mathbf{F}^i = \left[F_x^i, F_y^i \right]^T.$$

Recalling Fig. 3, the length of the hangers can be calculated by

$$h_i = y_{i+1} - y_{i+1}^d = y_i + \varphi_y^i - y_{i+1}^d \tag{28}$$

Substituting Eq. (8) and Eq. (28) into Eq. (9) leads to the

differential equation with respect to φ_y^i

$$\frac{\partial G_h^i}{\partial \varphi_y^i}=\frac{E_hA_h}{\sqrt{\left(E_hA_h+N_{i-1}\right)^2+2E_hA_hw_hh^{i-1}}}w_h=\gamma w_h \tag{29}$$

where $\gamma=\dfrac{E_hA_h}{\sqrt{\left(E_hA_h+N_{i-1}\right)^2+2E_hA_hw_hh^{i-1}}}$.

The relationship between $\Delta\mathbf{F}^i$ and $\Delta\mathbf{F}^{i-1}$ becomes according to Eq. (12)

$$\begin{aligned}\Delta\mathbf{F}^i&=\begin{bmatrix}1&0\\0&1\end{bmatrix}\Delta\mathbf{F}^{i-1}-\mathbf{w}\begin{bmatrix}\dfrac{\partial L_0^{i-1}}{\partial F_x^{i-1}},\dfrac{\partial L_0^{i-1}}{\partial F_y^{i-1}}\end{bmatrix}\Delta\mathbf{F}^{i-1}\\&-\gamma w_h\begin{bmatrix}0&0\\\dfrac{\partial \varphi_y^{i-1}}{\partial F_x^{i-1}}&\dfrac{\partial \varphi_y^{i-1}}{\partial F_y^{i-1}}\end{bmatrix}\Delta\mathbf{F}^{i-1}\\&=\begin{bmatrix}1&0\\-w\dfrac{\partial L_0^{i-1}}{\partial F_x^{i-1}}-\gamma w_h\dfrac{\partial \varphi_y^{i-1}}{\partial F_x^{i-1}}&1-w\dfrac{\partial L_0^{i-1}}{\partial F_y^{i-1}}-\gamma w_h\dfrac{\partial \varphi_y^{i-1}}{\partial F_y^{i-1}}\end{bmatrix}\Delta\mathbf{F}^{i-1}\end{aligned} \tag{30}$$

If neglecting the effect of the hanger elongation on the self-weight of the hanger, Eq. (9) can be simplified as

$$G_h^i=w_hh_0^i\approx w_hh^i \tag{31}$$

and thus the coefficient γ in Eq. (29) equals 1.

With the recursion relation expressed in Eq. (30), Eq. (26) can be simplified as

$$\mathbf{U}=\mathbf{U}\left(\mathbf{F}_m^1\right)+\left[\mathbf{J}\right]_{2\times2}\left[\Delta\mathbf{F}_m^1\right] \tag{32}$$

where, $\left[\mathbf{J}\right]_{2\times2}=\mathbf{C}_{2\times2n}\mathbf{F}_{2n\times2}$ and $\begin{bmatrix}\Delta\mathbf{F}_m^1\\\vdots\\\Delta\mathbf{F}_m^{2n}\end{bmatrix}=\mathbf{F}_{2n\times2}\Delta\mathbf{F}_m^1$.

According to Eq. (4), the following differential equation can be obtained

$$d\varphi_y=\frac{\partial \varphi_y}{\partial F_x}dF_x+\frac{\partial \varphi_y}{\partial F_y}dF_y+\frac{\partial \varphi_y}{\partial L_0}dL_0 \tag{33}$$

where

$$\frac{\partial \varphi_x}{\partial F_y}=\frac{\partial \varphi_y}{\partial F_x}=\frac{F_x}{w}\left(-\frac{1}{T_1}+\frac{1}{T_2}\right)$$

$$\frac{\partial \varphi_y}{\partial F_y}=-\frac{L_0}{EA}+\frac{1}{w}\left(-\frac{F_y}{T_1}+\frac{F_y-wL_0}{T_2}\right)$$

$$\frac{\partial \varphi_y}{\partial L_0}=-\frac{F_y}{EA}+\frac{wL_0}{EA}-\frac{F_y-wL_0}{T_2}$$

$$T_1=\sqrt{F_x^2+F_y^2}$$

$$T_2=\sqrt{F_x^2+\left(F_y-wL_0\right)^2}$$

Differentiating Eq. (3) respecting to F_x and L_0, respectively, lead to

$$\frac{\partial \varphi_x}{\partial F_x}=-\frac{L_0}{EA}-\frac{1}{w}\ln\frac{T_2-F_y+wL_0}{T_1-F_y}$$

$$+\frac{F_x^2}{w}\left[\frac{1}{T_1\left(T_1-F_y\right)}-\frac{1}{T_2\left(T_2-F_y+wL_0\right)}\right] \tag{34a}$$

$$\frac{\partial \varphi_x}{\partial L_0}=-\frac{F_x}{EA}-\frac{F_x}{T_2} \tag{34b}$$

When $\varphi_x=d_x$ is a constant, considering the implicit function and Eq. (3), the following relationships can be obtained

$$\frac{\partial L_0}{\partial F_x}=-\frac{\partial \varphi_x}{\partial F_x}/\frac{\partial \varphi_x}{\partial L_0} \tag{35a}$$

$$\frac{\partial L_0}{\partial F_y}=-\frac{\partial \varphi_x}{\partial F_y}/\frac{\partial \varphi_x}{\partial L_0} \tag{35b}$$

Substituting Eqs. (33)-(34) into Eq. (30) can achieve

$$\frac{d\varphi_y}{\partial F_x}=\frac{\partial \varphi_y}{\partial F_x}-\frac{\partial \varphi_y}{\partial L_0}\cdot\frac{\partial \varphi_x}{\partial F_x}/\frac{\partial \varphi_x}{\partial L_0} \tag{36a}$$

$$\frac{d\varphi_y}{\partial F_y}=\frac{\partial \varphi_y}{\partial F_y}-\frac{\partial \varphi_y}{\partial L_0}\cdot\frac{\partial \varphi_x}{\partial F_y}/\frac{\partial \varphi_x}{\partial L_0} \tag{36b}$$

The matrix $\mathbf{C}_{2\times2n}$ can be directly calculated from Eq. (36) and the matrix $\mathbf{F}_{2n\times2}$ can be calculated from Eq. (30) and Eqs. (35)-(36).

3.2 Sensitivity analysis

Fig. 5 shows a simplified single-span suspension bridge with a span of 120 m and 11 hangers, the sag-span ratio for the main cable is 1/10, and the area, density and elastic modulus of the cable are 0.08 m^2, 8.005×10^3 kg/m^3 and 2.00×10^{11} Pa, respectively. To validate the explicit flexible matrix derived in section 3.1, three loading cases are considered for calculating the Jacobian matrix.

Case 1: the cable only acts by its self-weight with neglecting the effect of the hangers and deck girder;

Case 2: the cable acts by its self-weight with concentrated load 5000 kN at each hanger shown in Fig. 5 while ignoring the effect of the hangers and stiffening girder;

Case 3: Only considering the load at each lower anchor of the hangers as 5000 kN with 0.01 m^2 for each hanger area and the same material as the main cable.

The obtained results are also compared with those calculated by FDM with different perturbation. Eq. (18) determines the initial load for calculating the flexible matrix. $\mathbf{F}_m^1=[-966.51,\ 386.61]^T$ kN for case 1, and $\mathbf{F}_m^1=[-73154.01,\ 29261.61]^T$ kN for case 2 and case 3.

Table 1 lists the sensitivities computed by FDM with different perturbations and by the proposed explicit method. The perturbation Δx_i is defined as a percentage between the variables in the FDM during the computations due to the value of the two variables are not at same magnitude. From Table 1, the sensitivities calculated by FDM vary with the perturbations and these sensitivities are not converging to those calculated by the proposed analytical method as perturbation Δx_i decreases. The optimal perturbation for this

Table 1 Sensitivities computed with the FDM and the proposed explicit method (Unit: m/N)

Cases		J_{ij}	J_{11}	J_{12}	J_{21}	J_{22}
Case 1	Finite difference method	Δx_i =1%	-1.13×10^{-5}	-5.91×10^{-5}	2.29×10^{-6}	-1.18×10^{-4}
		Δx_i =1×10^{-4} %	$\mathbf{-1.14\times10^{-5}}$	$\mathbf{-5.91\times10^{-5}}$	$\mathbf{2.35\times10^{-6}}$	$\mathbf{-1.18\times10^{-4}}$
		Δx_i =1×10^{-10} %	-1.14×10^{-5}	-5.91×10^{-5}	2.32×10^{-6}	-1.18×10^{-4}
		Δx_i =1×10^{-13} %	-2.11×10^{-5}	-9.42×10^{-5}	-2.02×10^{-5}	-9.65×10^{-4}
	Present work		$\mathbf{-1.14\times10^{-5}}$	$\mathbf{-5.91\times10^{-5}}$	$\mathbf{2.35\times10^{-6}}$	$\mathbf{-1.18\times10^{-4}}$
Case 2	Finite difference method	Δx_i =1%	-1.84×10^{-7}	-8.20×10^{-7}	-3.00×10^{-8}	-1.64×10^{-6}
		Δx_i =1×10^{-4} %	$\mathbf{-1.86\times10^{-7}}$	$\mathbf{-8.20\times10^{-7}}$	$\mathbf{-3.03\times10^{-8}}$	$\mathbf{-1.64\times10^{-6}}$
		Δx_i =1×10^{-10} %	-1.30×10^{-7}	-8.96×10^{-7}	-6.49×10^{-8}	-1.55×10^{-6}
		Δx_i =1×10^{-13} %	-3.90×10^{-8}	-8.10×10^{-5}	7.30×10^{-8}	-8.12×10^{-5}
	Present work		$\mathbf{-1.86\times10^{-7}}$	$\mathbf{-8.20\times10^{-7}}$	$\mathbf{-3.03\times10^{-8}}$	$\mathbf{-1.64\times10^{-6}}$
Case 3	Finite difference method	Δx_i =1%	1.84×10^{-7}	8.20×10^{-7}	3.04×10^{-8}	1.64×10^{-6}
		Δx_i =1×10^{-4} %	$\mathbf{1.86\times10^{-7}}$	$\mathbf{8.20\times10^{-7}}$	$\mathbf{3.07\times10^{-8}}$	$\mathbf{1.64\times10^{-6}}$
		Δx_i =1×10^{-10} %	1.95×10^{-7}	6.53×10^{-7}	3.24×10^{-8}	1.63×10^{-6}
		Δx_i =1×10^{-13} %	-3.25×10^{-5}	8.11×10^{-5}	-3.25×10^{-8}	1.62×10^{-4}
	Present work	γ	$\mathbf{1.85\times10^{-7}}$	$\mathbf{8.20\times10^{-7}}$	$\mathbf{2.99\times10^{-8}}$	$\mathbf{1.64\times10^{-6}}$
		γ=1	$\mathbf{1.85\times10^{-7}}$	$\mathbf{8.20\times10^{-7}}$	$\mathbf{2.99\times10^{-8}}$	$\mathbf{1.64\times10^{-6}}$

numerical example is $\Delta x_i=1\times10^{-4}$% where results calculated by the proposed method agrees well with almost all the sensitivities calculated by FDM under the three loading cases. By comparing with the analytical values, truncation errors still exist for 1% perturbation and the round-off errors are clearly visible when Δx_i smaller than 1×10^{-4}%. And when $\Delta x_i=1\times10^{-13}$%, the computed gradient matrix is incorrect. The effectiveness of the FDM depends on the perturbation Δx_i. For instance, the optimal perturbation is $\Delta x_i=1\times10^{-4}$% in this numerical example, however, it will change and it is difficult to select for other functions and calculation point. On the other hand, the proposed method can compute the analytical values directly, which gives a better choice compared with FDM.

In addition, the gradient matrix calculated with γ=1 is the same as that calculated with the actual γ determined by Eq. (30) from Case 3, this means that the self-weight of the hangers can be approximated by their deformed lengths during the gradient matrix derivation as for almost all suspension bridges the elongation of the hangers is small and the hangers should be in elastic state during operating period. The gradient matrix calculation procedure thus can be greatly simplified with γ equals 1.

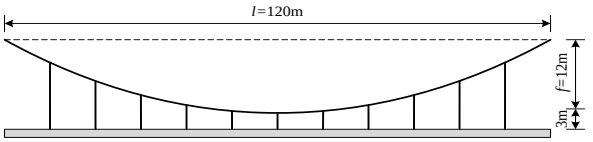

Fig. 5 A simplified cable structures

Table 2 Material and cross-sectional properties of the bridge

Structural member	E (Gpa)	A (m^2)	I (m^4)	w (kN/m)
Main span cable	210	0.4	-	32.9
Side span cable	210	0.41	-	33.8
Hanger	210	0.025	-	-
Deck	210	0.5	1.66	72.4

4. Numerical examples

Great Belt suspension bridge (Kim and Lee 2001) and Yingwuzhou Yangtze River Bridge *et al*. 2013) are investigated in order to show the efficiency of the improved analytical form-finding method in determining the initial shape of suspension bridges.

4.1 The Great Belt suspension bridge

For Great Belt suspension bridge, form-finding analysis has been performed by (Karoumi 1999), Kim and Lee (2001), Kim and Kim (2012). Fig. 6 shows the TCUD parameters and node number of the simplified Great Belt suspension bridge where the superstructure is supported by a roller on the cross beam of the pylons. The main cable is connected to the stiffening girder at the center of the bridge. In Fig. 6, the nodal points 1, 9, and 21 represent the position of the left spray saddle, tower saddle, and sag point at the center span with the predetermined y-coordinate of 0.00 m, 180.00 m and 0.001 m, respectively. Besides these, prior to a form-finding analysis, nodal coordinates for several structural points are also pre-determined for a target configuration as follows: 1) The hangers are vertically arranged and the camber of the deck girder was not considered; 2) The x-coordinates of nodal points at which the main cable and hangers interconnect are known; 3) The y-coordinates of nodal points at which the deck girder and hangers interconnect are 0.00 m. The other nodal coordinates are unknown parameters, for example, y-coordinates of main cable for the node no. 2-8 and 10-20, which shall be determined by a form-finding analysis.

Table 2 summarizes the material and cross-sectional properties of the bridge. As this bridge is an earth-anchored bridge, the axial forces and longitudinal displacement of the deck girder are not expected and the analytical method based form-finding analysis considers cable-only system, therefore the stiffness of the tower does not affect the form-finding analysis result and the parameters about the tower were not listed.

Table 3 summarizes the differences between the converged nodal coordinates of the main cable calculated by the proposed method, TCUD and I.TCUD methods. In Table 3, the third and the fourth columns were obtained

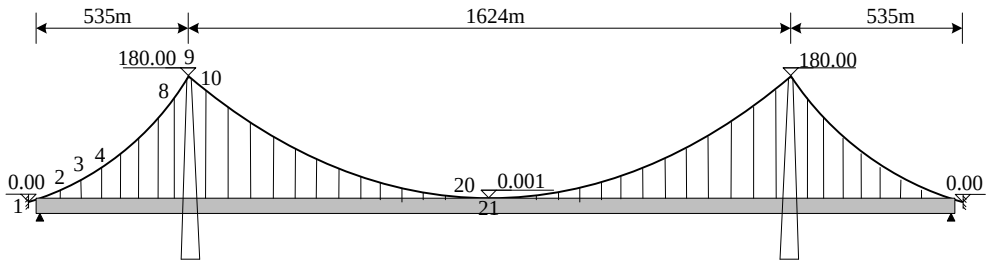

Fig. 6 Geometric parameters of the simplified suspension bridge

Table 3 Calculated nodal coordinates of the main cable

Node No.	x (m)	y (m)			(3)-(1)	(3)-(2)	Remarks
		(1) By TCUD	(2) By I.TCUD	(3) Present work	(m)	(m)	
1	0.000	**0.000**	**0.000**	**0.000**	0.000	0.000	main cable anchor
2	66.875	13.637	13.640	13.640	0.003	0.000	
3	133.750	29.967	29.973	29.974	0.007	0.001	
4	200.625	48.714	48.724	48.725	0.011	0.001	
5	267.500	69.961	69.975	69.976	0.015	0.001	
6	334.375	93.696	93.715	93.716	0.020	0.001	
7	401.250	119.935	119.959	119.961	0.026	0.002	
8	468.125	148.687	148.716	148.719	0.032	0.003	
9	535.000	**179.964**	**180.000**	**180.000**	0.036	0.000	tower saddle
10	602.667	151.101	151.132	151.129	0.028	-0.003	
11	670.333	124.787	124.812	124.811	0.024	-0.001	
12	738.000	101.011	101.032	101.031	0.020	-0.001	
13	805.667	79.764	79.781	79.780	0.016	-0.001	
14	873.333	61.038	61.050	61.050	0.012	0.000	
15	941.000	44.824	44.833	44.833	0.009	0.000	
16	1008.667	31.116	31.122	31.123	0.007	0.001	
17	1076.333	19.908	19.912	19.913	0.005	0.001	
18	1144.000	11.196	11.198	11.198	0.002	0.000	
19	1211.667	4.976	4.977	4.977	0.001	0.000	
20	1279.333	1.244	1.245	1.245	0.001	0.000	
21	1347.000	**0.001**	**0.001**	**0.001**	0.000	0.000	sag point

Table 4 Horizontal tension of the main cable ($\times 10^6$N)

Parameter	TCUD	I.TCUD	Present work
Horizontal tension of the main cable	194.00	193.75	193.69

from Kim and Kim (2012). The results from these three methods agree well with each other. However, the TCUD and I.TCUD methods require proper initial configuration estimation for the main cable ahead to ensure the convergence of the implementation and lead to challenge in engineering application. The convergence of the proposed method is independent of the initial configuration of the main cable. Therefore, the proposed analytical method has obvious advantages. Since the proposed method divides the bridge into two substructures and the form-finding analysis only refers to the cable system, the shortening of the main tower induced by the cable force does not affect the vertical coordinates of the main cable. However, the results calculated by TCUD illustrate that the vertical deformation of the tower leading to the actual sag of the main cable is 3.6 cm smaller than that of the other two methods. I.TCUD method can eliminate the deformation of the tower during the form-finding analysis by introducing initial force into the tower. The results calculated by the proposed method and I.TCUD agree well with each another. The maximum difference occurs at the two nodal points near the tower saddle with 3 mm. This difference may be resulted from that the proposed method is derived from the complete form of elastic catenary equations while the cable element in I.TCUD is derived from the linearized elastic catenary equations.

Table 4 shows that the three methods provide consistent results for the horizontal tension of the main cable. The maximum horizontal tension of the main cable occurs in the TCUD method. As discussed above, TCUD cannot eliminate the vertical deformation of the tower, which

Fig. 7 Yingwuzhou Yangtze River Bridge

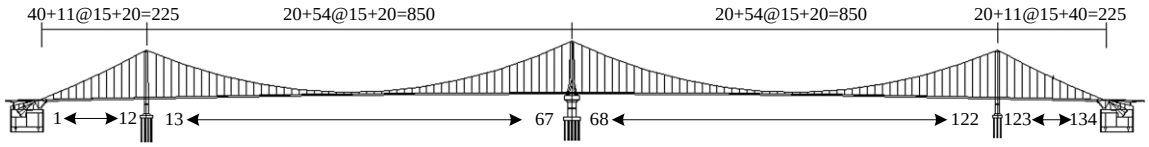

Fig. 8 Elevation view of Yingwuzhou Yangtze River Bridge (units in meters)

Fig. 9 The FE model of Yingwuzhou Yangtze River Bridge

implies the final mid-span sag will be smaller than the predetermined value as the tower deforms in vertical direction and leads to the increase in the horizontal force of the main cable.

4.2 Yingwuzhou Yangtze River Bridge

Yingwuzhou Yangtze River Bridge is employed to verify the applicability of the proposed method in large-scale real engineering application. As shown in Fig. 7, Yingwuzhou Yangtze River Bridge is the 8th bridge across the Yangtze River located in Wuhan with a span of (225+850+850+255) m. The total number of the hangers on each cable plane is 132, with 55 hangers in the main span and 11 hangers in each side span. Figure 8 shows the layout and number of the hangers. The cross sectional area, the cross sectional moment of transverse and vertical inertia of the stiffening girder are 1.563 m^2, 207.598 m^4, 1.105 m^4, respectively. The cross sectional area and elastic modulus of the main cable are 0.296 m^2, 2.05×10^{11} Pa, and the sag-span ratio of the main cable in main span is 1/9. The coordinates of the saddles on the three towers are (0, 0, 162.5), (±850, 0, 144.5) and that of the two anchors are (±1075, 0, 39.0). The dead load is 342.82 kN/m including the secondary dead load of 59.02 kN/m.

Generally speaking, an ideal suspension bridge FE model should satisfy the following three requirements: (1) the bridge's displacement under dead load equals to zero; (2) the calculated tension of the hangers should equal to that of the predetermined tension; (3) the calculated bending moment of the stiffness girder equals to that of calculated by the multi-support continuous beam model. In this analysis, these three points are considered as criterions to investigate the effectiveness of the proposed method.

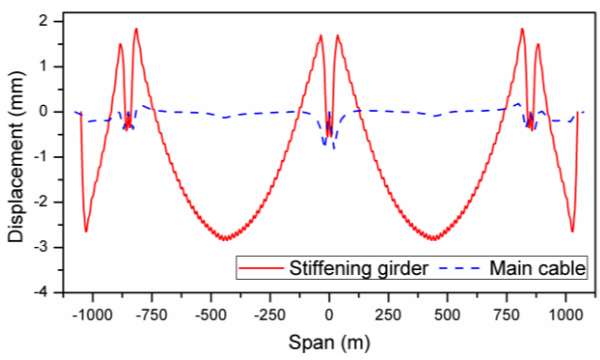

Fig. 10 Calculated displacement of the stiffening girder and main cable

Fig. 9 shows the FE model of the Yingwuzhou Yangtze River Bridge developed by Midas/Civil. Midas/Civil supplies elastic catenary cable element recognized as the most accurate element type to simulate the nonlinear properties of the cable elements. However, unlike beam or truss element, users need to define the initial tension or unstrained length for each cable element to calculate its stiffness matrix, which means the accuracy of the FE model highly depends on these initial tensions or unstrained lengths. As shown in Fig. 9, the FE model of Yingwuzhou Yangtze River Bridge contains 1619 nodes and 1601 elements, including 548 elastic catenary cable elements in total. The stiffness girder and tower are modeled by beam element while the main cable and the hangers utilize the catenary element. The nodal coordinate of the main cable and unstrained length of all catenary elements were calculated by the proposed form-finding approach. To eliminate the vertical deformation of the towers, proper initial forces equal to the internal forces induced by the

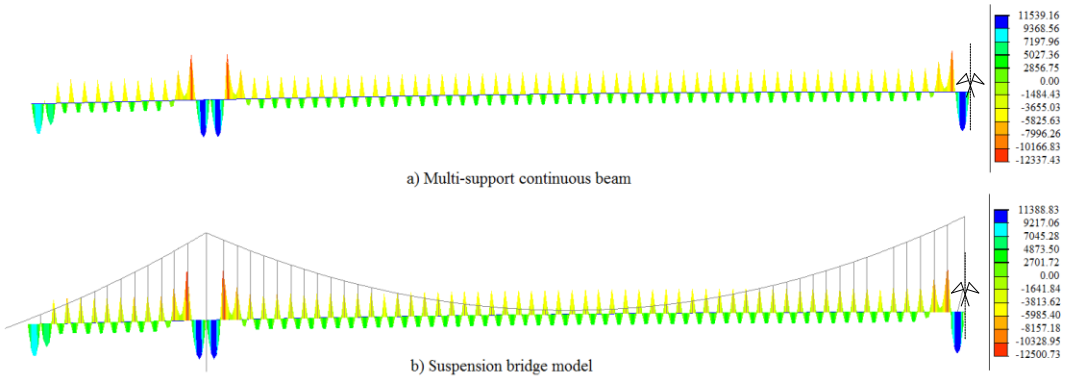

Fig. 12 Bending moment diagrams of the multi-support continuous beam and suspension bridge (kN.m)

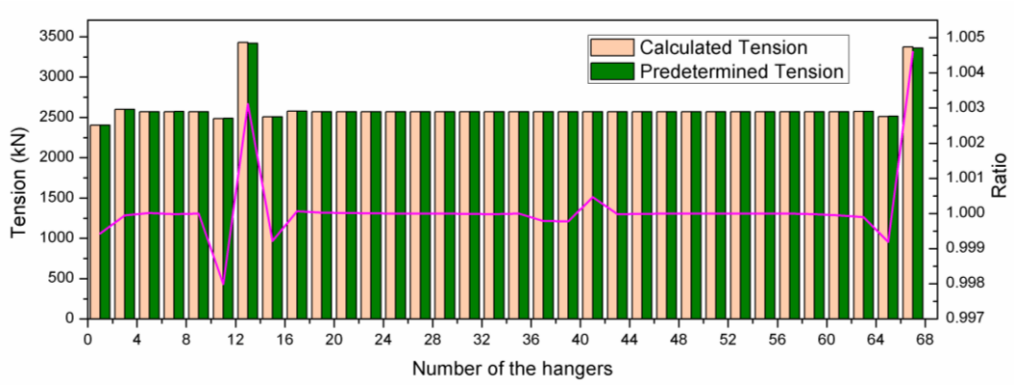

Fig. 11 Comparison of the calculated hanger tensions and the predetermined hanger tensions

main cable's compression to the towers have been introduced to the corresponding elements.

Fig. 10 demonstrates the displacement curves of the stiffening girder and main cable under dead load calculated from the FE model developed utilizing the results obtained by the form-finding analysis. The maximum displacement of the stiffening girder (smaller than 3 mm) occurs at the mid-span of each main span, and the maximum displacement of the main cable does not exceed 1 mm, which is much smaller compared with that of the stiffening girder. Fig. 11 shows the predetermined tensions of the odd numbered hangers from 1 to 67 calculated by the multi-support continuous model and that calculated from the FE model under dead load. The vertical label on the left side in Fig. 11 denotes the tension of the hanger and that on the right side shows the ratio of the calculated tension to predetermined tension. The line shows the variation of the tension ratio varies with different hangers. It shows that the maximum error of calculated hanger tensions is smaller than 0.5% of the predetermined tensions. Fig. 12 compares the bending moment of the stiffening girder calculated by the FE model and those yielded by the multi-support continuous beam model and the results agree well with each other, and the maximum error between them are less than 1.5%.

To summarize, the proposed method performs well in real bridge model and agrees well with the three criterions. The proposed method is an analytical method, where all the cable members' geometric parameters including nodal coordinates and unstrained lengths, were rigorously obtained from elastic catenary equations with no simplification in the deviation process. Meanwhile, the elastic catenary cable element supplied by Midas/Civil is derived from the linearized elastic catenary equations with neglecting the high-order terms of the equations that shall lead to errors between analytical method and FE method. Besides, the unavoidable error of the nonlinear solver of the FE software from round-off errors will also amplify these errors between the two different methods. In summary, the errors in the FE model developed by the proposed method are very small and acceptable and the form-finding method proposed in this paper can provide an accurate form-finding analysis result for suspension bridges.

5. Conclusions

This study addressed an explicit analytical iterative method for form-finding analysis in suspension bridge based on the gradient matrix derived from the differential form of the elastic catenary equations, where a sensitivity analysis is conducted for verification. Afterwards, two suspension bridges are investigated numerically to illustrate the accuracy and efficiency of the proposed form-finding analysis method. To conclude, following remarks can be obtained:

(1) An improved form-finding method is developed for accurate unstrained lengths calculation for the hangers based on the conventional analytical form-finding method. The Jacobian matrix for gradient-based

iteration algorithms is derived in an explicit form to overcome the inherent defects of FDM.

(2) The sensitivity analysis demonstrates that the gradient matrices calculated by the proposed method and by FDM with proper perturbations are consistent. The proposed method directly derives the accurate Jacobian matrix while FDM suffers both truncations errors and round-off errors.

(3) In the first example, the cable coordinates and horizontal tensions comparison between those obtained by the proposed analytical method and those derived by two NFEM-based form-finding methods confirms the accuracy and efficiency of the proposed method. The proposed method avoids the unfavorable influence induced by the shortening of towers compared with TCUD while the final results evaluated by it agrees well with those derived by I.TCUD.

(4) The proposed methodology shows capacity in the application of large-scale practical engineering structures from Yingwuzhou Yangtze River Bridge nonlinear FE analysis. In comparison with the fundamental criterions for suspension bridge, the maximum displacement error is smaller than 3 mm and the maximum relative error of hanger tensions and bending moment for the stiffening girder do not exceed 0.5% and 1.5%, respectively, which implies that the proposed method satisfies the requirements in engineering practice.

(5) The proposed method might be easily extended to spatial-shape cable from plane-shape cable and self-anchor suspension bridges that gives a promising future in real engineering application.

Acknowledgements

This research was supported by the Fundamental Research Funds for the Central Universities (WUT: 2015IVA015) and the National Natural Science Foundation of China (Grant No. 51408249). The authors would like to express their appreciation to A/Prof. Xudong Qian from National university of Singapore for discussions.

Reference

Cao, H., Chen, Z., Wu, Q., Zhu, H.P. and Kang, J. (2016), "A simplified model for multi-span suspension bridges based on single cable theory", *China J. Highw. Tran.*, **29**(4), 77-84.

Chen, Z., Cao, H., Ye, K., Zhu, H. and Li, S. (2013), "Improved particle swarm optimization-based form-finding method for suspension bridge installation analysis", *J. Comput. Civil Eng.*, **29**(3), 04014047.

Chen, Z., Cao, H. and Zhu, H. (2015), "An iterative calculation method for suspension bridge's cable system based on exact catenary theory", *Baltic J. Road Bridge Eng.*, **8**(3), 196-204.

Chen, Z., Cao, H., Zhu, H., Hu, J. and Li, S. (2014), "A simplified structural mechanics model for cable-truss footbridges and its implications for preliminary design", *Eng. Struct.*, **68**, 121-133.

Fan, L., Pan, Y. and Du, G. (1999), "Study on the fine method of calculating the erection-parameters of long-span suspension bridges", *Chin Civil Eng. J.*, **32**, 20-25.

Faroughi, S., Kamran, M.A. and Lee, J. (2014), "A Genetic algorithm approach for 2-D tensegrity form finding", *Adv. Struct. Eng.*, **17**(11), 1669-1679.

Gimsing, N.J. and Georgakis, C.T. (2011), *Cable Supported Bridges: Concept and Design*, John Wiley & Sons.

Irvine, H.M. (1981), *Cable Structures*, The MIT Press, Cambridge.

Jung, M.R., Min, D.J. and Kim, M.Y. (2013), "Nonlinear analysis methods based on the unstrained element length for determining initial shaping of suspension bridges under dead loads", *Comput. Struct.*, **128**, 272-285.

Jung, M.R., Min, D.J. and Kim, M.Y. (2015), "Simplified analytical method for optimized initial shape analysis of self-anchored suspension bridges and its verification", *Math. Prob. Eng.*, **2015**, Article ID 923508, 14.

Karoumi, R. (1999), "Some modeling aspects in the nonlinear finite element analysis of cable supported bridges", *Comput. Struct.*, **71**(4), 397-412.

Kim, H.K. and Kim, M.Y. (2012), "Efficient combination of a TCUD method and an initial force method for determining initial shapes of cable-supported bridges", *Int. J. Steel Struct.*, **12**(2), 157-174.

Kim, H.K., Lee, M.J. and Chang, S.P. (2002), "Non-linear shape-finding analysis of a self-anchored suspension bridge", *Eng. Struct.*, **24**(12), 1547-1559.

Kim, K.S. and Lee, H.S. (2001), "Analysis of target configurations under dead loads for cable-supported bridges", *Comput. Struct.*, **79**(29), 2681-2692.

Kim, M.Y., Kim, D.Y., Jung, M.R. and Attard, M.M. (2014), "Improved methods for determining the 3 dimensional initial shapes of cable-supported bridges", *Int. J. Steel Struct.*, **14**(1), 83-102.

Koohestani, K, and Guest, S.D. (2013), "A new approach to the analytical and numerical form-finding of tensegrity structures", *Int. J. Solid. Struct.*, **50**(19), 2995-3007.

Lonetti, P, and Pascuzzo, A. (2014), "Optimum design analysis of hybrid cable-stayed suspension bridges", *Adv. Eng. Softw.*, **73**, 53-66.

Lund, E. (1994), "Finite element based design sensitivity analysis and optimization", Institute of Mechanical Engineering, Aalborg University, Denmark.

Luo, X.H. (2004), "Numerical analysis method for cable system of suspension bridges", *J. Tongji Univ.*, **4**, 5.

O'Brien, T. (1967), "General solution of suspended cable problems", *J. Struct. Div.*, **93**(1), 1-26.

O'Brien, W.T. and Francis, A.J. (1964), "Cable movements under two-dimensional loads", *ASCE J. Struct. Div*., **90**, 89-123.

Sun, Y., Zhu, H.P. and Xu, D. (2014), "New method for shape finding of self-anchored suspension bridges with three-dimensionally curved cables", *J. Bridge Eng.*, **20**(2), 04014063.

Sun, Y., Zhu, H.P. and Xu, D. (2016), "A specific rod model based efficient analysis and design of hanger installation for self-anchored suspension bridges with 3D curved cables", *Eng. Struct.*, **110**, 184-208.

Wang, P.H. and Yang, C.G. (1996), "Parametric studies on cable-stayed bridges", *Comput. Struct.*, **60**(2), 243-260.

Wang, S., Zhou, Z., Gao, Y. and Huang, Y. (2015), "Analytical calculation method for the preliminary analysis of self-anchored suspension bridges", *Math. Prob. Eng.*, **2015**, Article ID 918649, 12.

Wriggers, P. (2008), *Nonlinear Finite Element Methods*, Springer Science & Business Media.

Zhang, L.Y., Li, Y., Cao, Y.P. and Feng, X.Q. (2014), "Stiffness matrix based form-finding method of tensegrity structures", *Eng. Struct.*, **58**, 36-48.

CC